CrossMark

A novel hierarchical graphene/polyaniline hollow microsphere as electrode material for supercapacitor applications

Ling Liu[1], Yan Wang[1], Qinghan Meng[1,*], and Bing Cao[1]

[1] *The Key Laboratory of Beijing City on Preparation and Processing of Novel Polymer Materials, Beijing University of Chemical Technology, Beijing 100029, China*

ABSTRACT

A hierarchical graphene/polyaniline hollow microspheres with sandwich structure (GCS@PANI@RGO) have been successfully synthesized by the in situ polymerization of PANI on the surface of graphene carbon sphere (GCS) and then the electrostatic self-assembly of graphene oxide and reduction without etching templates. The morphologies and microstructures of the microspheres were characterized by scanning electron microscopy, X-ray diffraction, Fourier transform infrared spectroscopy, X-ray photoelectron spectroscopy, energy-dispersive X-ray spectroscopy and nitrogen adsorption measurements. The results show that the GCS@PANI@RGO composites demonstrate desirably hierarchical hollow microspheres with sandwich structure and the strong interactions such as electrostatic interactions, hydrogen bonding and π–π interactions existed between the layers in hierarchical hollow microspheres. The electrochemical behaviors of GCS@PANI@RGO as electrode were investigated by cyclic voltammograms, galvanostatic charge–discharge and electrochemical impedance spectroscopy. The GCS@PANI-8@RGO showed a high specific capacitance of 446.19 F g^{-1} at the scanning rate of 5 mV s^{-1} in 1 M H$_2$SO$_4$ solution, and exhibit an outstanding long-term cycling stability with capacitance retentions of 93.4% after 1000 charging–discharging cycles at a current density of 2 A g^{-1} and even 88.7% after 5000 cycles. The excellent electrochemical performance can be ascribed to the novel sandwiched hollow structure, and the synergic effect of the three components of GCS, PANI and RGO, which greatly enhance the electrical conductivity, promote the utilization of active materials and improve the structural stability. Therefore, such novel hierarchical hollow materials could be considered as quite suitable and promising electrodes for high-performance supercapacitors.

Address correspondence to E-mail: qhmeng@mail.buct.edu.cn

⚡ Springer

Introduction

With the rapid development of the global economy, electronic technology has dramatically progressed during the past few decades. At the same time, the resource exhaustion and the environmental contamination urgently require to develop new sustainable and reliable energy storage and conversion technologies, such as rechargeable batteries, fuel cells, and supercapacitors [1, 2]. Supercapacitors, also known as electrochemical capacitors (EC), have attracted increasing interest owing to their unique properties including high power density, fast charge–discharge rates, super rate capability and long life cycle [3–5]. Generally, energy storage mechanisms are classified into two categories: faradaic pseudo-capacitances and electrical double-layer capacitances (EDLC) [6]. The EDLC derives from reversible ion adsorption at the electrode interface of the active materials such as carbon materials, while the capacitance of pseudocapacitors arises from the faradic transformation or reversible redox on the electrode surface of capacitive materials such as conductive polymers [7]. Carbon materials such as carbon nanotubes, activated carbon and graphene are commonly used as the attractive electrode materials due to their good electric conductivity, excellent stability and large specific surface area [8]. In particular, graphene, as an intriguing two-dimensional single-atom-thick carbon material, has attracted tremendous attention for its theoretical specific surface area up to 2630 $m^2\ g^{-1}$, high carrier mobility at room temperature approaching 10,000 $cm^2\ V^{-1}\ S^{-1}$, good optical transmittance about 97.7% and Young's modulus of 1.0 TPa [9–12]. On the other hand, among the pseudocapacitive materials, polyaniline (PANI) is one of the most promising electrode materials because of its environmental stability, simple synthesis, low cost, high electrical conductivity, interesting redox properties and great capacitance for energy storage [13, 14]. Unfortunately, due to its swelling, cracks and shrinkage, PANI exhibits an inferior cycle life and fast degraded capacitance during high-rate cycling processes [15, 16]. Therefore, in order to alleviate these limitations, the combination of PANI with carbon materials has been recognized as an effective way to improve the capacitance value and the cycling stability with synergistic effects [17, 18]. Various types of graphene/PANI composite structures have been designed and synthesized by different methods to further improve the electrochemical performance [7–9, 19–25].

Hollow micro-/nanostructured materials have received considerable attention and been recognized as one type of promising material for high-performance electrical energy storage devices [20]. Because the hollow-structured material with inner cavity and pore structures can enhance the specific surface area and shorten diffusion length for both charge and mass transport [21, 22]. Luo et al. [23] prepared graphene-PANI hybrid hollow spheres by utilizing polystyrene (PS) spheres as sacrificial template via electrostatic interaction and layer-by-layer assembly technique. And after 1000 charging/discharging cycles, capacitance retentions of 83% were maintained. Choi et al. [24] synthesized the novel

Scheme 1 Schematic of synthetic route of the hierarchical graphene/PANI hollow microspheres.
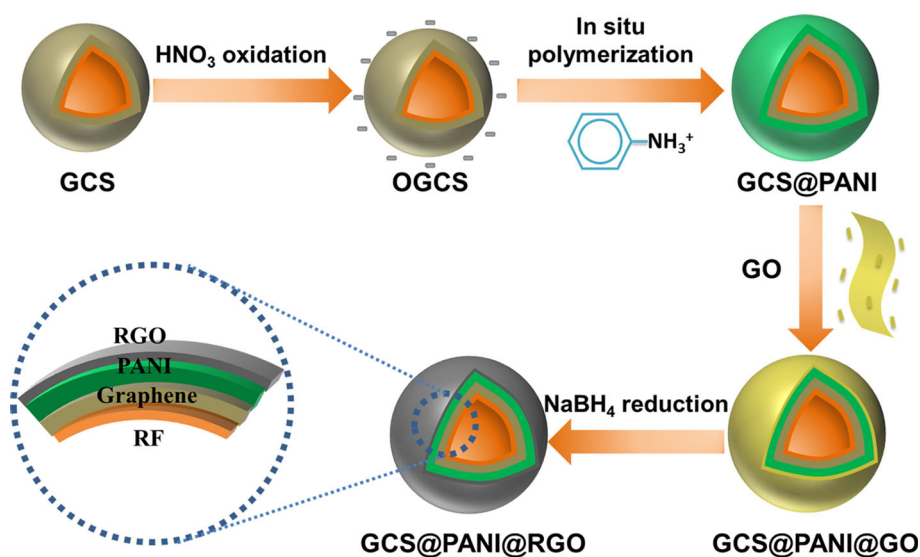
graphene-PANI hybrid hollow balls. The polymethyl methacrylate (PMMA) colloidal particles were used as a template, through the self-assembly of graphene oxide (GO), the situ polymerization of polyaniline and removal of the PMMA core by etching in chloroform to obtain the final three-dimensional (3D) hollow balls of graphene and PANI composites, with a 14% loss of capacitance after 500 cycles. Liu et al. [25] fabricated graphene-wrapped polyaniline hollow spheres using PS spheres as templates by a solution-based coassembly method and electrochemical reduction, which retained 90% of its initial capacitance after 500 cycles. Despite these substantial progresses, actually the above researches used the polymer as template methods to prepare hollow spheres, and then the template was etched by corrosive solvents such as chloroform or tetrahydrofuran, which is impractical due to the tedious process, high cost and high energy consumption [26, 27]. Besides, the removal of the templates usually brings some bad effects on the electrochemical performance. To the best of our knowledge, the synthesis of sandwiched graphene/PANI hollow microspheres without etching templates possess has not been reported.

In this paper, a novel hierarchical graphene/PANI hollow microsphere with sandwich structure was successfully synthesized without etching templates. The synthesis route of the novel materials is illustrated in Scheme 1. Firstly, graphene carbon sphere (GCS) as basic scaffold was synthesized using the GO, resorcinol and formaldehyde (RF) by inverse suspension polymerization and pyrolysis, which showed high specific area and long-term cycling stability as electrode materials. Subsequently, the GCS was treated by nitric acid to obtain the oxidized GCS spheres (OGCS), which had negative charge on the surface. Then, OGCS/PANI composites (GCS@PANI) were fabricated by electrostatic interactions and in situ polymerization of aniline on the OGCS. Finally, the GO was wrapped on the surface of GCS@PANI spheres through electrostatic self-assembly and reduced to graphene (RGO) by a reduction reaction and then the hierarchical graphene/PANI hollow microspheres (GCS@PANI@RGO) with sandwich structure were obtained. The morphologies and microstructures of the microspheres were characterized by scanning electron microscopy (SEM), X-ray diffraction (XRD), Fourier transform infrared spectroscopy (FTIR), X-ray photoelectron spectroscopy (XPS), energy-dispersive X-ray spectroscopy (EDX) and nitrogen adsorption measurements. The electrochemical property of GCS@PANI@RGO as electrode materials for EC was investigated by cyclic voltammograms (CV), galvanostatic charge–discharge (GCD) and electrochemical impedance spectroscopy (EIS). The results demonstrate that the capacitance was maintained at 93.4% after 1000 charging–discharging cycles at a current density of 2 A g^{-1} and even 88.7% after 5000 cycles, indicating that the novel hierarchical hollow microsphere could be a promising candidate as electrode material for high-performance supercapacitor applications.

Experimental section

Materials

Natural graphite powder (G, 325 meshes) and aniline (An, $\geq$99.5 wt%) were purchased from Sigma-Aldrich. Ammonium persulfate (APS, 98.0% purity), sodium borohydride (NaBH$_4$, $\geq$98.0% purity), H$_2$SO$_4$ (95–98 wt%), Cyclohexane($\geq$99.5 wt%) and HCl (36–38 wt%) were from Beijing Chemical Co., Ltd. (China). All commercial chemicals were used as received without further purification. The deionized (DI) water used throughout all the experiments was purified by a Pgeneral pure water system in our laboratory.

Preparation of GO

GO was prepared from graphite powder using a modified Hummers method [28]. Typically, the as-prepared GO particles are negatively charged in aqueous solutions and the concentration of the GO solution used here was about 0.5 mg mL^{-1}.

Preparation of GCS

The GCS was prepared according to the method reported in our previous work [29]. In brief, the GCS was prepared using the GO and RF by inverse suspension polymerization under ambient pressure drying and carbonization at 800 °C in a nitrogen atmosphere for 2 h.

Preparation of OGCS

Then, the as-prepared GCS spheres were dispersed in 60 mL of 4 mol L^{-1} nitric acid and the oxidation

reaction was allowed to take place at 90 °C for 6 h under refluxing conditions. The OGCS spheres were finally obtained by centrifugation, rinsed with a large amount of distilled water and dried for the further use.

Preparation of GCS@PANI hollow microspheres

Growth of PANI on the surface of OGCS was performed by a modified in situ polymerization method according to previous literature [30] to prepare the GCS@PANI composites. In a typical procedure, 0.3 g of An was dispersed in the 100-mL HCl (1 M) aqueous solution containing 10 mL ethanol solution. A 0.2 g OGCS was added into the above solution, and the mixture was kept under magnetic stirring for 4 h at 0–5 °C to allow the swelling process and absorption of aniline hydrochloride on the surface of the GCS spheres. An aqueous solution of APS (50 mL HCl (1 M) aqueous solution containing 5 mL ethanol solution, 1:1 molar ratio of APS to aniline) was slowly dropped into the mixture. The polymerization was allowed to proceed in ice bath for 2, 4, 6, 8 and 10 h with stirring, and the resulting composites with the varying reaction time were denoted as GCS@PANI-2, GCS@PANI-4, GCS@PANI-6, GCS@PANI-8 and GCS@PANI-10, respectively. The precipitate was washed with ethanol and distilled water in order to remove residual reactants and byproducts completely, and dried at 50 °C under vacuum for 24 h.

Preparation of GCS@PANI@RGO hollow microspheres

Hundred milligrams of GCS@PANI was dispersed in 100 mL of water, which are positively charged in aqueous solutions. The GO solution was gradually added to the above solution under stirring for 2 h to prepare the GCS@PANI@GO composites (GCS@PANI/GO 10:1 wt/wt) via electrostatic interactions. Then, 0.1 g of sodium borohydride ($NaBH_4$) was added into the mixture solution and stirred at 90 °C for 2 h. The reduced composite was washed by rinsing and centrifugation with deionized water for several times to remove excess $NaBH_4$. The resulting material was dispersed in 1 M HCl solution containing APS and stirred at room temperature overnight for the reoxidation and reprotonation of PANI. Finally, the as-prepared product was washed with

distilled water and dried at 50 °C in an oven. The products were identified as GCS@PANI-2@RGO, GCS@PANI-4@RGO, GCS@PANI-6@RGO, GCS@PANI-8@RGO and GCS@PANI-10@RGO.

Characterization

The morphologies of the samples were observed using SEM (Hitachi S-4700, Japan) under the operating voltage of 20 kV, which equipped with an energy-dispersive X-ray spectroscopy (EDX) system. The functional groups and crystal structures of composites were characterized by FTIR (PerkinElmer Spectrum RX1, USA) and XRD (BrukerAXS D8 ADVANCE, Germany). The elemental composition on the sample surface was investigated by XPS (Thermo Electron Corporation ESCALAB 250, USA). The surface area and pore volume were measured by N_2 adsorption using an adsorption apparatus (Micromerities ASAP 2020, USA).

Electrochemical measurements

All electrochemical tests were carried out in N_2-saturated 1 M H_2SO_4 aqueous solution at room temperature. The working electrode was stainless steel mesh pasted with a homogeneous mixture of the hybrid hollow microsphere with acetylene black and binder (polytetrafluoroethylene, PTFE) at a mass ratio of 80:10:10. CV and EIS were tested using an electrochemical work station (Zahner-Elektrik, Germany) in a three-electrode system. A square platinum plate and a saturated calomel electrode (SCE) were used as the counter and reference electrodes, respectively. The CV tests were performed in the potential range of −0.2–0.8 V (vs. SCE). The EIS measurements were recorded at 10 mHz to 100 kHz and an alternating current (ac) voltage amplitude of 5 mV peak-to-peak. GCD experiments were measured by the Arbin BT-4 battery tester (USA) with the voltage range of 0–0.8 V in a two-electrode system.

Results and discussion

SEM images analysis

Figure 1 exhibits the SEM images of GCS, GCS@PANI-8 and GCS@PANI-8@RGO. As shown in Fig. 1a, d, the surface of GCS is clean and slight
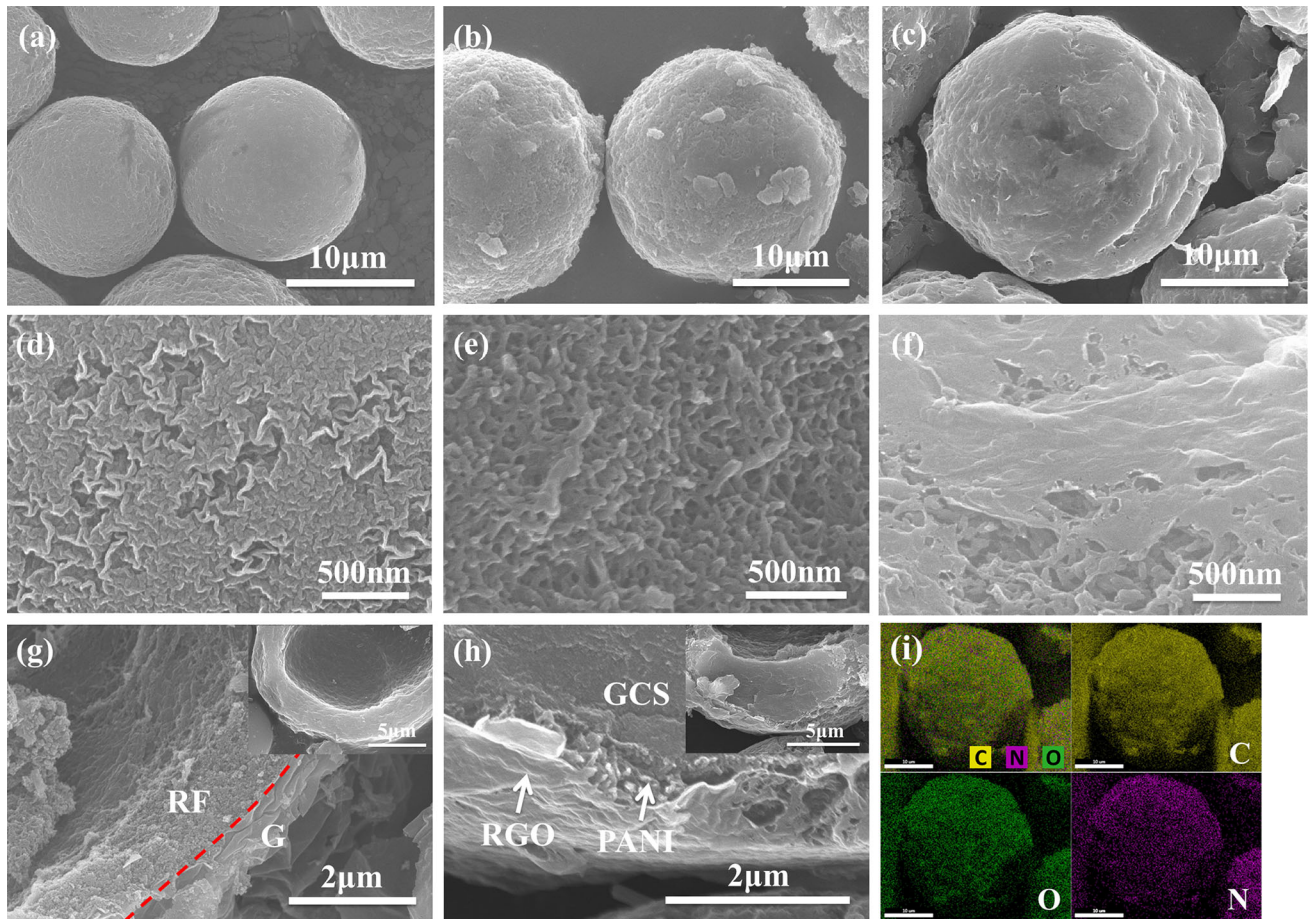
Figure 1 SEM images of **a** GCS, **b** GCS@PANI-8, **c** GCS@PANI-8@RGO; the surface of **d** GCS, **e** GCS@PANI-8, **f** GCS@PANI-8@RGO in high magnification; the lateral view of the **g** GCS shell, **h** GCS@PANI-8@RGO shell, **i** EDX mapping for GCS@PANI-8@RGO.

wrinkle, caused by the pleated graphene sheets. After the in situ polymerization of PANI, the surface of the GCS@PANI-8 microspheres (Fig. 1b) obviously becomes rougher and the size is larger than that of the GCS. Ordered nanofiber morphology can be clearly observed in the GCS@PANI-8 (Fig. 1e), indicating that the PANI has successfully grown on the surface of the GCS. The combination of porous GCS with PANI has been formed, which are beneficial to the electrolyte infiltration and ion transmission. After the introduction of GO via electrostatic interactions into the GCS@PANI-8, the GCS@PANI-8@RGO microspheres (Fig. 1c) become much larger than GCS@PANI-8, with diameters about 20 μm. The flexible graphene layer can be obviously seen in Fig. 1f, wrapping on the GCS@PANI spheres.

In addition, the lateral views of microspheres are observed in Fig. 1g, h, which further clearly confirms they are hierarchical hollow structures. According to the side view of the GCS shells (Fig. 1g), the outer layer of microsphere is wrinkled graphene sheets, and the inner layer consists of RF particles. As shown in Fig. 1h, the PANI layers with nanofiber morphology and the well-defined graphene layers are observed and they are tightly adhered on the GCS substrate. The thickness of GCS@PANI-8@RGO microsphere shell is about 4 μm. The result shows that the hierarchical graphene/PANI hollow microsphere with sandwich structure has been successfully synthesized. Figure 1i shows the EDX mapping taken from the GCS@PANI-8@RGO microsphere. The N element from PANI can be clearly observed in the EDX mapping, further confirming that the hierarchical structure of GCS@PANI@RGO, which is in agreement with the results of the SEM.

The SEM images of PANI and GCS@PANI composites with varying reaction time of PANI are shown in Fig. 2. The pure PANI (Fig. 2a) shows
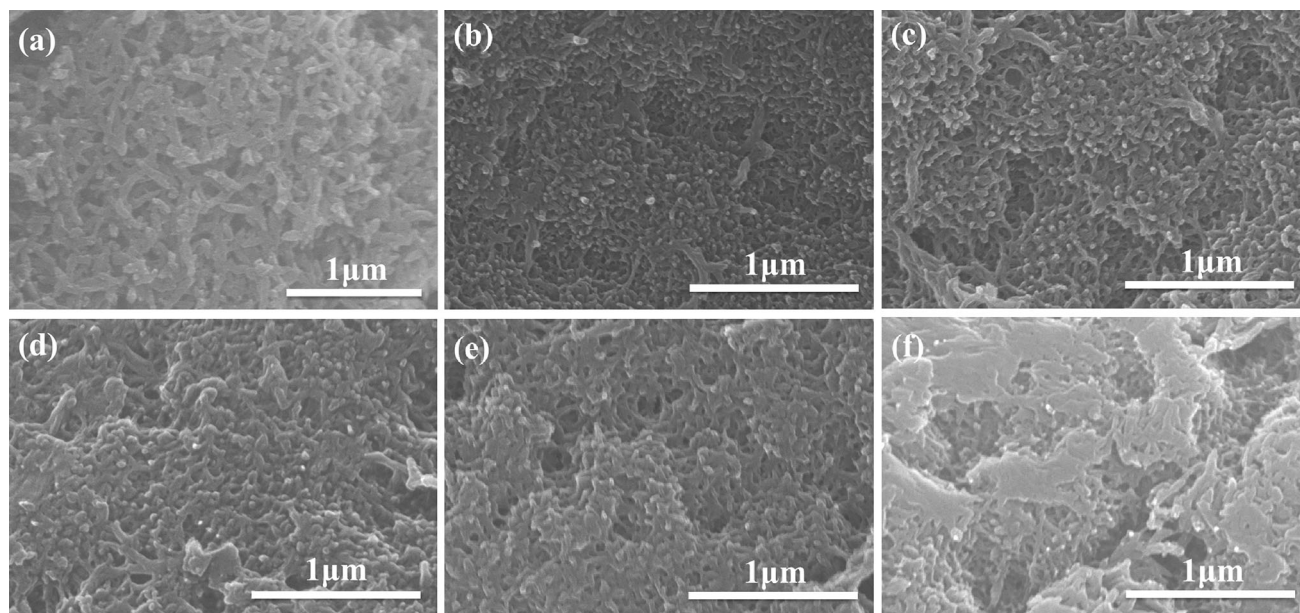
Figure 2 SEM images of **a** PANI, **b** GCS@PANI-2, **c** GCS@PANI-4, **d** GCS@PANI-6, **e** GCS@PANI-8, **f** GCS@PANI-10 surface.

disorderly stacking nanofiber morphology, while all GCS@PANI samples exhibit relatively regular morphology than pure PANI. For the GCS@PANI-2 (Fig. 2b), PANI nanofibers with the length smaller than 100 nm are formed. With the increase in reaction time, the length of the nanofibers also increases. From the SEM image of GCS@PANI-8 (Fig. 2e), it can be seen that the length of PANI nanofibers is about 250 nm. For GCS@PANI-10 (Fig. 2f), the nanofiber structure becomes compact and nonuniform, due to the occurrence of excessive oxidation can lead to a breakdown of the polymer chain [31], which is disadvantage to the electrolyte infiltration and diffusion. Consequently, a suitable polymerization time of PANI is important to achieve a uniform PANI structure.

FTIR spectra analysis

The FTIR spectra of OGCS, PANI, RGO, GCS@PANI and GCS@PANI@RGO are shown in Fig. 3. For RGO, peak at 1580 cm^{-1} reflects the skeletal vibration of graphene sheets [32]. From the spectrum of the OGCS, the absorption bands at 1720 cm^{-1} reflect the C=O stretching vibrations in carboxylic acid [33], indicating that the negative charge has existed in the GCS. The bands centered at 1537 and 1225 cm^{-1} are attributed to the aromatic C=C and epoxy functional groups, respectively [34, 35]. For GCS@PANI-8, the absorption peaks at 796, 1135, 1296, 1492 and

1569 cm^{-1} are ascribed to the aromatic C–H inside and outside bending vibration of the 1,4-disubstituted aromatic ring, C–N stretching of the second amine, C=C stretching of the benzenoid rings and C=C stretching of the quinoid ring, respectively [36], which is similar to characteristic bands of pure PANI. The disappearance of peak at 1720 cm^{-1} of the OGCS is due to that the carboxyl groups on the surface of OGCS can be connected to N atoms in PANI as a proton doping agent electrostatic interactions [37]. The result suggests the aniline has successfully
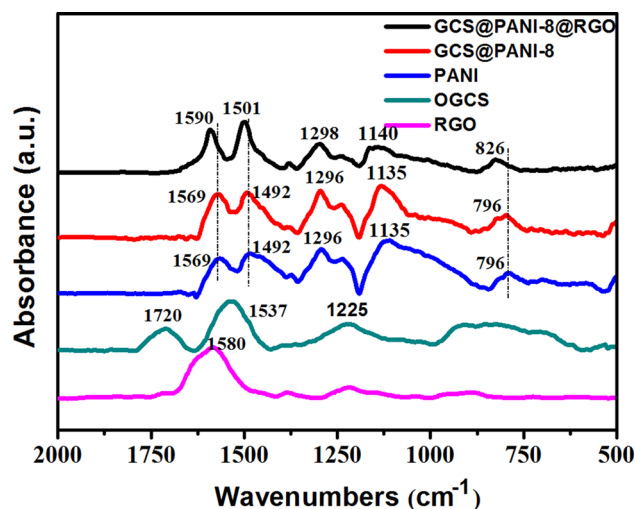

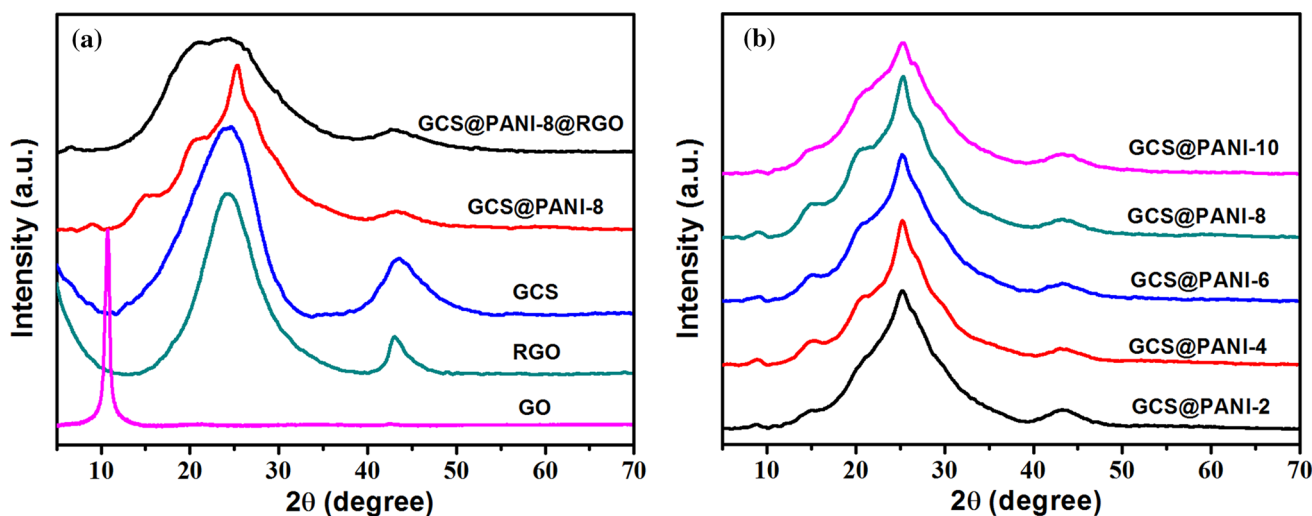**Figure 3** FTIR spectra of OGCS, PANI, RGO, GCS@PANI-8, GCS@PANI-8@RGO.

Figure 4 XRD patterns of **a** GO, RGO, GCS, GCS@PANI-8 and GCS@PANI-8@RGO, **b** GCS@PANI composites.

adsorbed and polymerized on the surface of the GCS by electrostatic interactions. After electrostatic self-assembly of GO and a reduction reaction, the peaks at 826, 1140, 1298, 1501 and 1590 cm^{-1} that belong to PANI are still observed in the GCS@PANI-8@RGO, demonstrating the PANI exists in the composite. Furthermore, comparing the GCS@PANI-8 with RGO, the peaks for GCS@PANI-8@RGO composite are shifted slightly to higher frequencies, resulting from the strong multiple interactions between the GCS@PANI and RGO, such as electrostatic interactions, hydrogen bonding and π–π interactions [35, 38, 39], which means that RGO layers are well wrapped the GCS@PANI sphere.

XRD analysis

Figure 4a presents the XRD patterns of GO, RGO, GCS, GCS@PANI-8 and GCS@PANI-8@RGO composites. It can be observed that GO shows a typical peak at $2\theta = 10.76°$, corresponding to the diffraction of (001) pattern [40]. After $NaBH_4$ reduction, a broad peak with peak (002) at $2\theta = 24.22°$ and a narrow peak (100) at $2\theta = 42.98°$ were detected, indicating the successful preparation of RGO [41]. The diffraction peaks of GCS are similar to those of RGO, but it is broader than that of RGO. For the GCS@PANI-8 sample, 8.94°, 14.96°, 20.84° and 25.3° correspond to (001), (011), (020) and (200) characteristic crystal planes of doping PANI, respectively [42, 43]. The peak at 43.28° can be attributed to (100) graphite-like structure caused by GCS [44]. The result means that

the PANI has grown on the surface of GCS. The XRD patterns of GCS@PANI composites with varying reaction time are shown in Fig. 4b. Diffraction peaks of all samples are similar, and the intensities gradually increase from GCS@PANI-2 to GCS@PANI-8. The GCS@PANI-8 has strongest diffraction peak, indicating more regular crystalline structures [45], which is consistent with the SEM investigations. Interestingly, the GCS@PANI-8@RGO shows a broad and intense diffraction peak from 10° to 35° corresponding to the (020) planes of PANI and some weak reflections. The broad peak results from the overlap with the diffractions from RGO and GCS@PANI-8 [46], indicating the strong interactions and conjugation between the GCS@PANI-8 and RGO. Therefore, the XRD result further confirms the strong interactions between the layers in hierarchical hollow microspheres.

XPS analysis

The chemical composition of GCS@PANI-8 and GCS@PANI-8@RGO was further determined by XPS analysis (see Fig. 5). The predominant elements (Fig. 5a) are detected in the GCS@PANI-8 and GCS@PANI-8@RGO samples with peaks at about 285 eV (C 1s), 400 eV (N 1s) and 532 eV (O 1s), respectively [47], suggesting the presence of PANI in the GCS@PANI-8 and GCS@PANI-8@RGO. According to the XPS data, the surface nitrogen content decreases from 3.2% of GCS@PANI-8 to 1.62% of GCS@PANI-8@RGO, which indicates the surface of
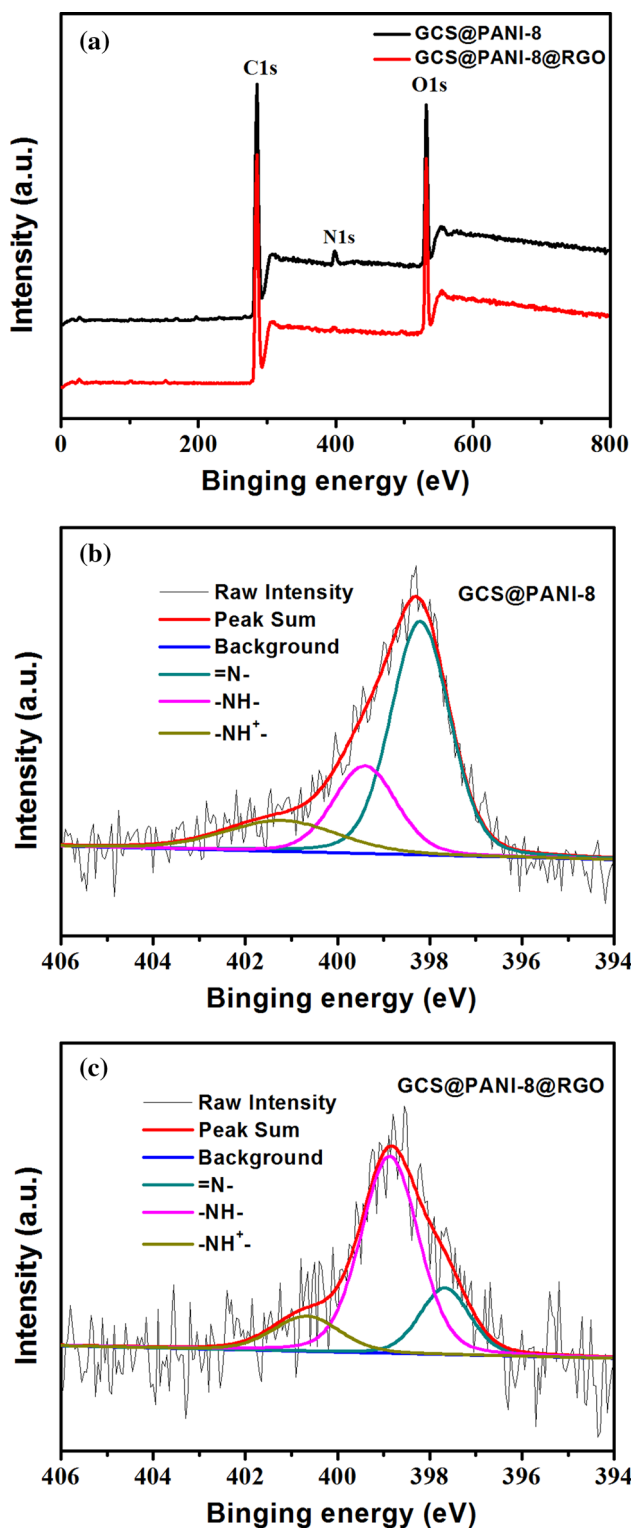
Figure 5 a XPS spectra of GCS@PANI-8 and GCS@PANI-8@RGO, **b** the N 1*s* XPS spectra of GCS@PANI-8, **c** the N 1*s* XPS spectra of GCS@PANI-8@RGO.

GCS@PANI-8 has been covered by the RGO. In the XPS of GCS@PANI-8 (Fig. 5b), the N 1*s* spectra are split into three peaks at 398.2, 399.5 and 401.2 eV, corresponding to quinonoid amine (=N–), benzenoid amine (–NH–) and nitrogen cationic radical (–NH$^+$–), respectively [48, 49]. For GCS@PANI-8@RGO (Fig. 5c), the N 1*s* spectrum can be deconvoluted into three peaks with binding energies of 397.7, 398.8 and 400.7 eV, which is slightly decreasing than that of GCS@PANI-8. The small decrease in electronic binding energies can be attributed to the hydrogen bond and π–π interaction between graphene and PANI chains [47, 50], which may facilitate the charge transfer and bring a synergistic effect to the electrochemical performance of the microspheres.

Nitrogen adsorption measurements analysis

The texture of the GCS and GCS@PANI-8@RGO was investigated by the N$_2$ adsorption. From the shape of the N$_2$ adsorption–desorption isotherm (Fig. 6a) and the pore size distribution plot (Fig. 6b), it can be deduced that the GCS predominantly represents the mesopores and micropores [51]. The specific surface area of GCS is calculated to be 536.7 m^2 g^{-1} by the Brunauer–Emmett–Teller (BET) measurement. For the GCS@PANI-8@RGO (Fig. 6c), a linear increase in the lower pressure range is due to the monolayer adsorption of N$_2$ molecules in the micro- and mesopores. An obvious hysteresis loop appears in the pressure range of P/P$_0$ = 0.4–0.9, indicating the existence of mesopores. The sharp uptakes in P/P$_0$ = 0.9–1.0 can be ascribed to the macroporous structure [52]. The macropores are formed by the inter-particle voids and the gaps from PANI fibers and graphene at outer layer. Figure 6d exhibits the pore size distribution of GCS@PANI-8@RGO centered from 1.4 to 32 nm. The specific surface area of GCS@PANI-8@RGO is decreased to 113.8 m^2 g^{-1}, which is due to some pore blockage after wrapping PANI and graphene. Similar results also have been reported in previous researches [8, 53]. The hierarchical microsphere of GCS@PANI-8@RGO integrating micropores, mesopores and macropores is beneficial for the fast transport of electrolyte ions and enhances the electrochemical properties.
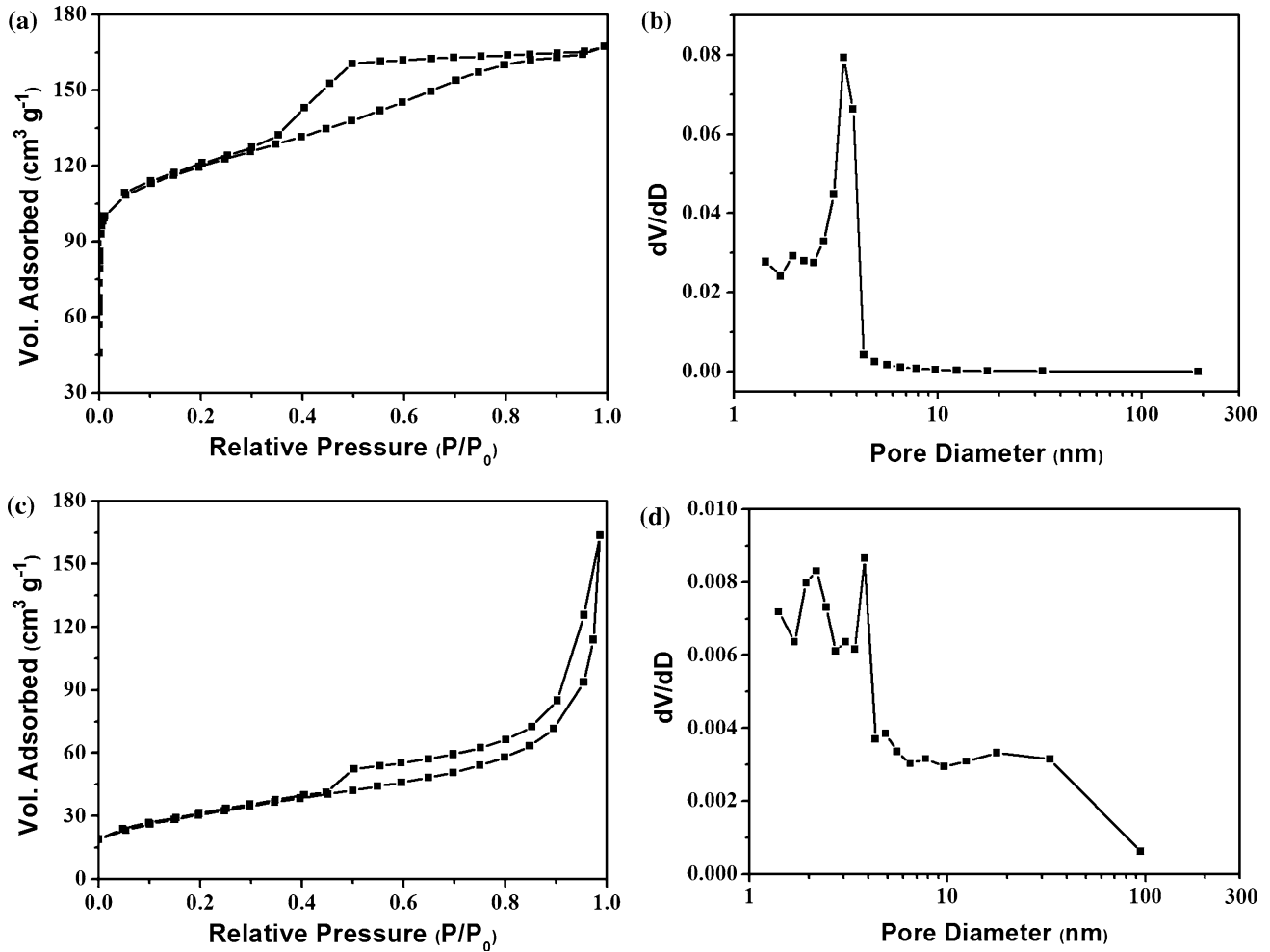
Figure 6 a Nitrogen adsorption/desorption isotherm and **b** pore size distribution of GCS, **c** Nitrogen adsorption/desorption isotherm and **d** pore size distribution of GCS@PANI-8@RGO.

## Electrochemical performance analysis

The electrochemical performances of all the GCS@PANI@RGO are analyzed by CV, EIS and GCD tests. The corresponding CV curves at the scanning rate of 5 mV s^{-1} are shown in Fig. 7a. All curves exhibit two couples of redox peaks (0.24 V/0 V, 0.50 V/0.42 V), which are caused, respectively, by the redox transitions of leucoemeraldine form and faradic transformation of emeraldine or from its emeraldine and pernigraniline [54]. The CV curve of GCS@PANI-8@RGO shows a largest encircling area than other samples, indicating a higher specific capacitance. The high capacitance of the GCS@PANI-8@RGO can be attributed to its novel hierarchical hollow structure, regular PANI nanofiber morphology and the synergistic effect between graphene and PANI nanofibers, which can ensure a good charge propagation, a high utilization of PANI and effective ion adsorption in the electrode materials. The specific capacitances based on the CV tests (C_{CV}) can be calculated from Eq. (1).

$$C_{CV} = \frac{1}{mv(V_b - V_a)} \int_{V_a}^{V_b} I dv \qquad (1)$$

where C_{CV} (F g^{-1}) is the specific capacitance derived from CV tests, I (A) is the current response of the potential, V_b (V) is the maximum voltage and V_a (V) the minimum voltage of the CV tests, v (V s^{-1}) is the potential scan rate and m (g) is the weight of the electroactive materials in the electrodes.

According to the above formula, from GCS@PANI-2@RGO to GCS@PANI-10@RGO, the specific capacitance is 291.32, 328.42, 403.74, 446.19 and 373.72 F g^{-1}, respectively. The lower capacitance of GCS@PANI-10@RGO is probably due to the existence
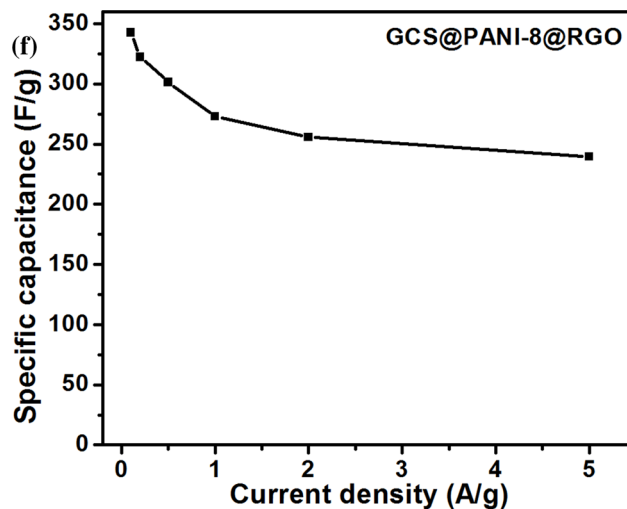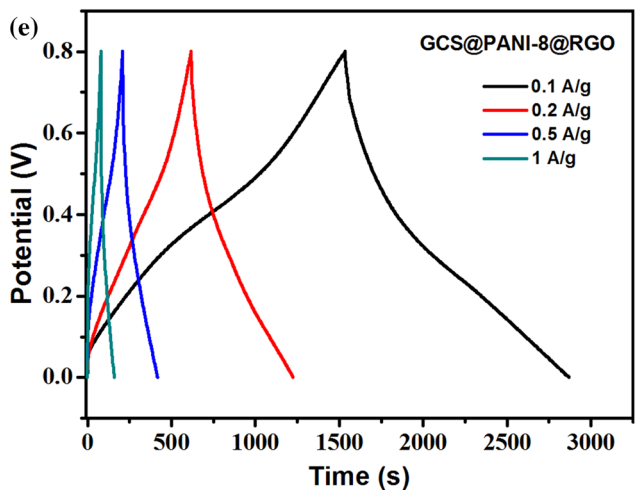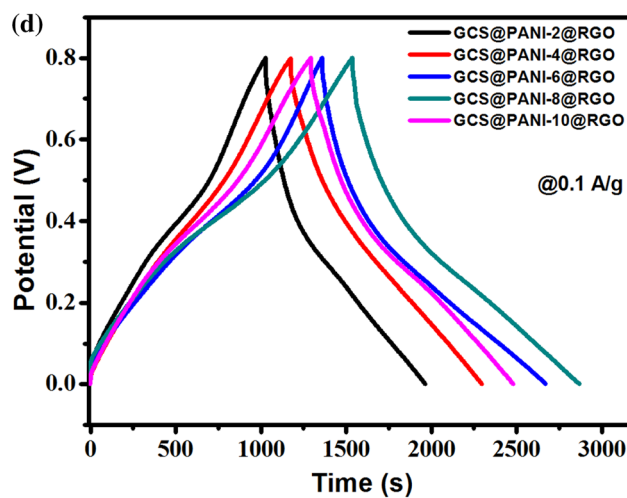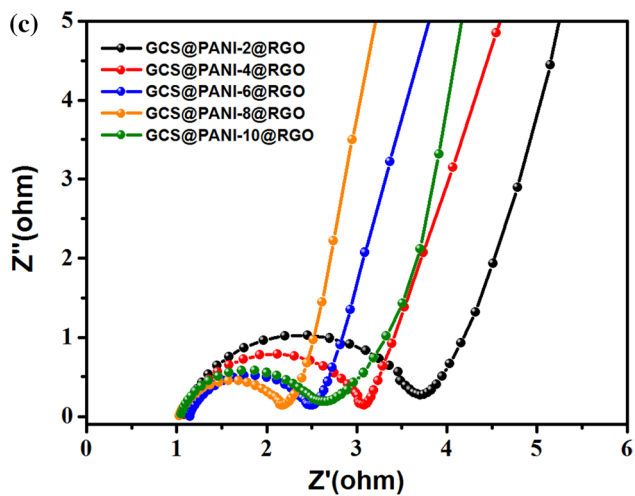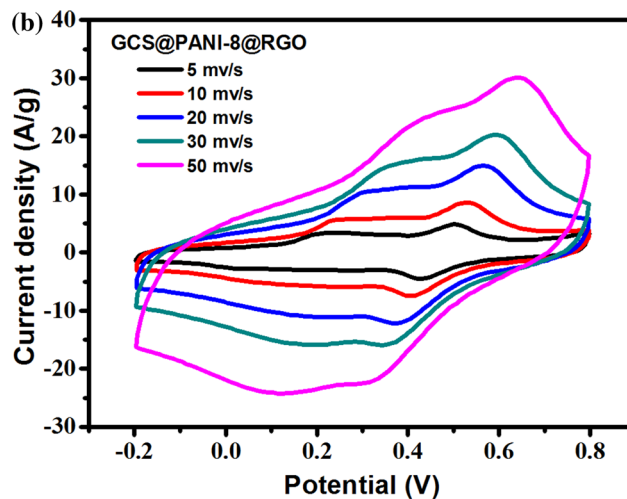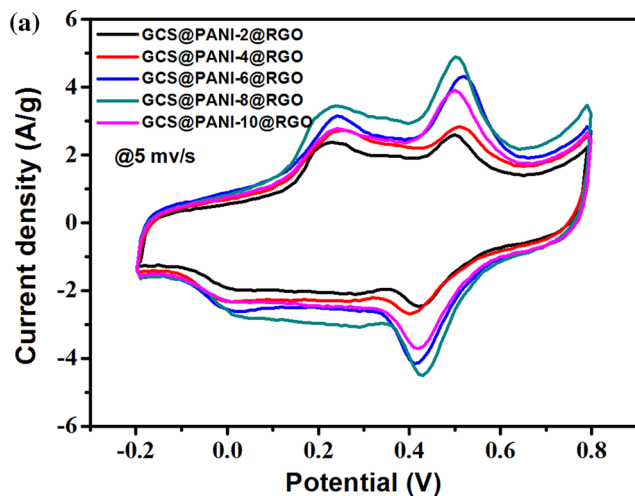
◀**Figure 7** Electrochemical properties for GCS@PANI@RGO materials **a** CV curves measured at a scan rate of 5 mV s^{-1}, **b** CV curves of GCS@PANI-8@RGO composite electrode measured at different scan rates, **c** Nyquist plots of composite electrodes; **d** GCD curves measured at a current density of 0.1 A g^{-1}, **e** GCD curves of GCS@PANI-8@RGO composite electrode measured at different current densities, **f** Plots of specific capacitance for GCS@PANI-8@RGO at different current densities.

of compact and disordering PANI nanofibers in the sample, which is disadvantage to the electrolyte infiltration and ion transmission. Similar results have been demonstrated in previous reports [30, 31]. Figure 7b shows the CV curves of the GCS@PANI-8@RGO composites at different scan rates. It can be observed that the CV curves almost maintain the same shape with the increasing scan rates, indicating the rapid redox reaction of GCS@PANI-8@RGO. This implies that the GCS@PANI-8@RGO composite has excellent electrical conductivity and a quick mass transfer capability as electrode.

The EIS (Fig. 7c) was used to analyze the electrochemical frequency behavior of the capacitor system. In the high frequency region, the semicircle intercept with the real axis is the equivalent series resistance (ESR) of the interfacial charge transport resistance, the electrolyte solution and the intrinsic resistance of the active material [55]. All the samples show comparable ESR around 1 Ω. The semicircle size is related to the interfacial charge transport resistance, the variation of which is consistent with specific capacitance. At low frequency, the slope of 45° portion of

the curve is related to Warburg resistance resulting from the electrolyte ion diffusion behavior, while vertical portion indicates pure capacitive behavior [56, 57]. It can be seen that the straight line of GCS@PANI-8@RGO is more perpendicular to X axis, showing a better capacitor performance and lower diffusion resistance of ions in electrolyte.

The GCD curves of GCS@PANI@RGO hybrid hollow spheres at the current density of 0.1 A g^{-1} are shown in Fig. 7d. All of the samples display a bent triangular shape, and the discharge curves exhibit two voltage stages in the ranges of 0.8–0.4 and 0.4–0 V, which are associated with the double-layer capacitance and a combination of double-layer and pseudocapacitive capacitance, respectively [58, 59]. It is obvious that discharge time of GCS@PANI-8@RGO is longer than other samples, which can be indicated that the material has lower energy consumption from the internal resistance and higher efficiency of energy storage. The rate performance of GCS@PANI-8@RGO is also evaluated by GCD tests at an increasing current density, as displayed in Fig. 7e, f. At different current densities, the curves are still kept linear and symmetrical and 69% of its initial capacitance is maintained with the current density increasing from 0.1 to 5 A g^{-1}, suggesting that the electrode material has excellent electrochemical reversibility and charge/discharge performance [59].

The cycling performance of materials is another important parameter used to determine the electrodes for practical application. The cycling experiment of GCS@PANI-8@RGO is evaluated at a current density of 2 A g^{-1}. As shown in Fig. 8a, there is no obvious
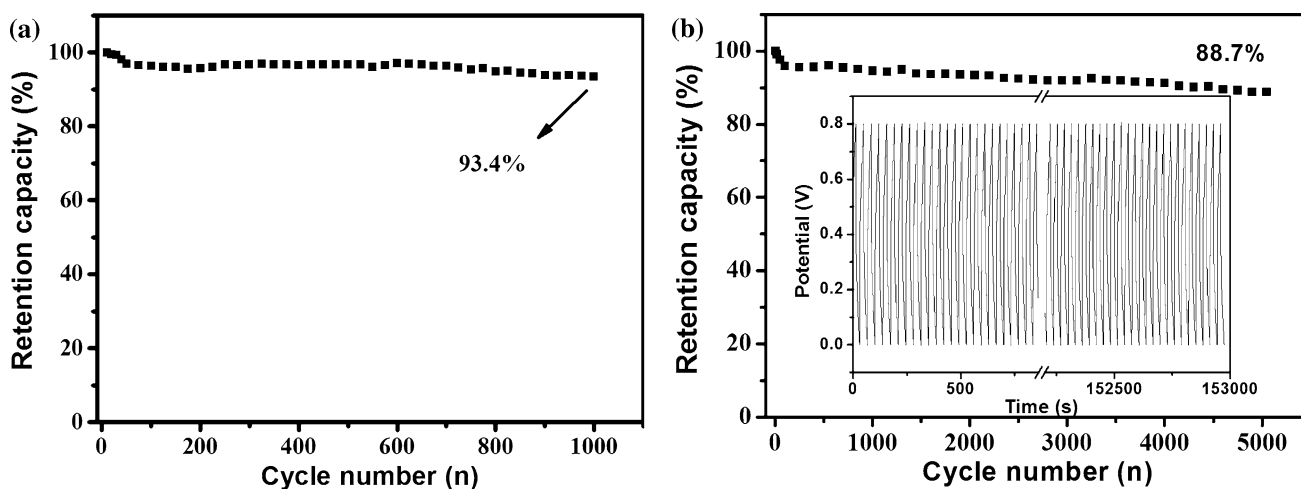

Figure 8 Cycling stability test of GCS@PANI-8@RGO composite electrode: **a** 1000 cycles, **b** 5000 cycles.

Table 1 Comparison of electrochemical performances of the reported graphene/polyaniline hollow microspheres as supercapacitors and the present work

Samples	Specific capacitances (F g^{-1})	Cycling performance	Reference
Nanostructured polystyrene/polyaniline/reduced graphene oxide hybrid materials	180 (0.5 A g^{-1})	74% after 5000 cycles (6 A g^{-1})	5
Graphene–polyaniline hybrid hollow spheres (using PS spheres as templates)	456 (0.5 A g^{-1})	83% after 1000 cycles (0.5 A g^{-1})	23
Graphene-PANI hybrid hollow balls (PMMA as templates)	331 (1 A g^{-1})	86% after 500 cycle (1 A g^{-1})	24
Graphene-wrapped polyaniline hollow (PS spheres as templates)	614 (1 A g^{-1})	90% after 500 cycle (1 A g^{-1})	25
Reduced graphene oxide–polyaniline hollow spheres (PS spheres as templates)	752 (1 A g^{-1})	92% after 1000 cycle (1 A g^{-1})	36
Hierarchical graphene/polyaniline hollow microsphere (without etching templates)	446.19 (5 mV s^{-1})	93.4% after 1000 cycle (2 A g^{-1}) and 88.7% after 5000 cycle	This work

decrease after 1000 cycle, and 93.4% of the initial capacitance is retained. Even after 5000 cycles (Fig. 8b), 88.7% of the initial capacitance is still maintained, which is better than those of previous reports (as listed in Table 1). The better period stability is mainly ascribed to unique hierarchical hollow architecture. In the sandwiched material, GCS acts as a basic scaffold for PANI and RGO, at the same time GCS can offer higher surface area, providing high electroactive regions, short diffusion lengths and lower ion-transport resistance. The introduction of PANI into the composites offers highly conductive pathways by bridging between adjacent GCS and RGO, so significantly facilitates electrolyte ion penetration for fast electron transfer. Finally, the RGO layers wrapped on the GCS@PANI serves as physical buffering layers or networks to inhibit the swelling and shrinking of PANI during the charge–discharge process, which maintain the structural integrity [7, 30]. As a result, we believe that GCS@PANI-8@RGO is a quite suitable and promising electrode material for high-performance supercapacitors.

Conclusions

In summary, hierarchical GCS@PANI@RGO hollow microspheres with sandwich structure have been successfully synthesized by the in situ polymerization of PANI on the surface of GCS and then the electrostatic self-assembly of GO and reduction. From the SEM images, the GCS@PANI@RGO composites demonstrate desirably hierarchical hollow microspheres with sandwich structure. The diameter is about 20 μm, and the wall thickness is about 4 μm. The FTIR, XRD and XPS spectra confirmed that the strong interactions such as electrostatic interactions, hydrogen bonding and π–π interactions existed between the layers in hierarchical hollow microspheres. The novel sandwiched hollow structure and the synergic effect of the three components of GCS, PANI and RGO greatly enhance the electrical conductivity, promote the utilization of active materials and improve the structural stability, resulting in excellent electrochemical properties. The GCS@PANI-8@RGO shows a high specific capacitance of 446.19 F g^{-1} at the scanning rate of 5 mV s^{-1} in 1 M H_2SO_4 solution. Furthermore, the GCS@PANI-8@RGO as electrode materials has a good long-term cycling stability, and the capacitance is maintained at 88.7% after 5000 charging–discharging cycles at a current density of 2 A g^{-1}. Therefore, it could be considered as quite suitable and promising electrodes for high-performance supercapacitors.

References

[1] Chauhan NPS, Mozafari M, Chundawat NS, Meghwal K, Ameta R, Ameta SC (2016) High-performance supercapacitors based on polyaniline-graphene nanocomposites: Some approaches, challenges and opportunities. Ind Eng Chem 36:13–29

[2] Wang G, Zhang L, Zhang J (2012) A review of electrode materials for electrochemical supercapacitors. Chem Soc Rev 41:797–828

[3] Mu B, Liu P, Wang A (2013) Synthesis of polyaniline/carbon black hybrid hollow microspheres by layer-by-layer assembly used as electrode materials for supercapacitors. Electrochim Acta 88:177–183

[4] Tan YB, Lee J-M (2013) Graphene for supercapacitor applications. J Mater Chem A 1:14814–14843

[5] Chen J, Liu Y, Li W, Wu C, Xu L, Yang H (2015) Nanostructured polystyrene/polyaniline/graphene hybrid materials for electrochemical supercapacitor and Na-ion battery applications. J Mater Sci 50:5466–5474. doi:10.1007/s10853-015-9092-z

[6] Pandolfo AG, Hollenkamp AF (2006) Carbon properties and their role in supercapacitors. J Power Sour 157:11–27

[7] Liu X, Wen N, Wang X, Zheng Y (2015) A high-performance hierarchical graphene@polyaniline@graphene sandwich containing hollow structures for supercapacitor electrodes. ACS Sustain Chem Eng 3:475–482

[8] Lei Z, Chen Z, Zhao XS (2010) Growth of polyaniline on hollow carbon spheres for enhancing electrocapacitance. J Phys Chem C 114:19867–19874

[9] Wang L, Lu X, Lei S, Song Y (2014) Graphene-based polyaniline nanocomposites: preparation, properties and applications. J Mater Chem A 2:4491–4509

[10] Ke Q, Wang J (2016) Graphene-based materials for supercapacitor electrodes-a review. J Materiomics 2:37–54

[11] Kopelevich Y, Esquinazi P (2007) Graphene physics in graphite. Adv Mater 19:4559–4563

[12] Lee C, Wei X, Kysar JW, Hone J (2008) Measurement of the elastic properties and intrinsic strength of monolayer graphene. Science 321:385–388

[13] Hui Z, Sun Y, Geng L, Chen S, Yun L (2014) Interfacial assembly and electrochemical properties of nafion-modified-graphene/polyaniline hollow spheres. Polymer 55:4459–4467

[14] Sestrem RH, Ferreira DC, Landers R, Temperini MLA, Nascimento GMD (2010) Synthesis and spectroscopic characterization of polymer and oligomers of ortho-phenylenediamine. Eur Polym J 46:484–493

[15] Frackowiak E, Khomenko V, Jurewicz K, Lota K, Béguin F (2006) Supercapacitors based on conducting polymers/nanotubes composites. J Power Sour 153:413–418

[16] Snook GA, Kao P, Best AS (2011) Conducting-polymer-based supercapacitor devices and electrodes. J Power Sour 196:1–12

[17] Yu T, Zhu P, Xiong Y, Chen H, Kang S, Luo H, Guan S (2016) Synthesis of microspherical polyaniline/graphene composites and their application in supercapacitors. Electrochim Acta 222:12–19

[18] Luo J, Chen Y, Ma Q, Liu R, Liu X (2014) Layer-by-layer assembled ionic-liquid functionalized graphene-polyaniline nanocomposite with enhanced electrochemical sensing properties. J Mater Chem C 2:4818–4827

[19] Wang Y, Yang X, Qiu L, Li D (2013) Revisiting the capacitance of polyaniline by using graphene hydrogel films as a substrate: the importance of nano-architecturing. Energ Environ Sci 6:477–481

[20] Fan W, Xia Y-Y, Weng WT, Pallathadka PK, He C, Liu T (2013) Nitrogen-doped graphene hollow nanospheres as novel electrode materials for supercapacitor applications. J Power Sour 243:973–981

[21] Wang JG, Yang Y, Huang ZH, Kang F (2012) Interfacial synthesis of mesoporous MnO_2/polyaniline hollow spheres and their application in electrochemical capacitors. J Power Sour 204:236–243

[22] Yang W, Gao Z, Song N, Zhang Y, Yang Y, Wang J (2014) Synthesis of hollow polyaniline nano-capsules and their supercapacitor application. J Power Sour 272:915–921

[23] Luo J, Ma Q, Gu H, Zheng Y, Liu X (2015) Three-dimensional graphene-polyaniline hybrid hollow spheres by layer-by-layer assembly for application in supercapacitor. Electrochim Acta 173:184–192

[24] Trung NB, Tam TV, Kim HR, Hur SH, Kim EJ, Choi WM (2014) Three-dimensional hollow balls of graphene-polyaniline hybrids for supercapacitor applications. Chem Eng J 255:89–96

[25] Fan W, Zhang C, Tjiu WW, Pramoda KP, He C, Liu T (2013) Graphene-wrapped polyaniline hollow spheres as novel hybrid electrode materials for supercapacitor applications. ACS Appl Mater Interfaces 5:3382–3391

[26] Lai X, Halpert JE, Wang D (2012) Recent advances in micro-/nano-structured hollow spheres for energy applications: From simple to complex systems. Energ Environ Sci 5:5604–5618

[27] Xu W, Mu B, Zhang W, Wang A (2016) Facile fabrication of well-defined polyaniline microtubes derived from natural kapok fiber for supercapacitor with long-term cycling stability. RSC Adv 6:68302–68311

[28] Tian G, Liu L, Meng Q, Cao B (2014) Facile synthesis of laminated graphene for advanced supercapacitor electrode material via simultaneous reduction and N-doping. J Power Sour 274:851–861

[29] Liu L, Liao L, Meng Q, Cao B (2015) High performance graphene composite microsphere electrodes for capacitive deionization. Carbon 90:75–84

[30] Cao H, Zhou X, Zhang Y, Chen L, Liu Z (2013) Microspherical polyaniline/graphene nanocomposites for high performance supercapacitors. J Power Sour 243:715–720

[31] Rao PS, Sathyanarayana DN, Palaniappan S (2002) Polymerization of aniline in an organic peroxide system by the inverted emulsion process. Macromolecules 35:4988–4996

[32] Lian P, Zhu X, Liang S, Li Z, Yang W, Wang H (2010) Large reversible capacity of high quality graphene sheets as an anode material for lithium-ion batteries. Electrochim Acta 55:3909–3914

[33] Liu L, Yang J, Meng Q (2013) Graphene cross-linked phenol-formaldehyde hybrid organic and carbon xerogel during ambient pressure drying. J Sol–Gel Sci Technol 66:1–5

[34] Bao L, Li X (2012) Towards textile energy storage from cotton T-shirts. Adv Mater 24:3246–3252

[35] Gao S, Zhang LI, Qiao Y, Dong P, Shi J, Cao S (2016) Electrodeposition of polyaniline on threedimensional graphene hydrogel as a binder-free supercapacitor electrode with high power and energy densities. RSC Adv 6:58854–58861

[36] Jiu H, Huang C, Zhang L, Chang J, Jiao H, Zhang S, Jia WB (2015) Excellent electrochemical performance of graphene-polyaniline hollow microsphere composite as electrode material for supercapacitors. J Mater Sci: Mater Electron 26:8386–8393. doi:10.1007/s10854-015-3505-2

[37] Yang N, Zhai J, Wan M, Wang D, Jiang L (2010) Layered nanostructures of polyaniline with graphene oxide as the dopant and template. Synthetic Met 160:1617–1622

[38] Dai W, Ma L, Gan M, Wang S, Sun X, Wang H, Zhou T (2015) Fabrication of sandwich nanostructure graphene/ polyaniline hollow spheres composite and its applications as electrode materials for supercapacitor. Mater Res Bull 76:344–352

[39] Wei H, Zhu J, Wu S, Wei S, Guo Z (2013) Electrochromic polyaniline/graphite oxide nanocomposites with endured electrochemical energy storage. Polymer 54:1820–1831

[40] Marcano DC, Kosynkin DV, Berlin JM, Sinitskii A, Sun Z, Slesarev A, Alemany LB, Lu W, Tour JM (2010) Improved synthesis of graphene oxide. ACS Nano 4:4806–4814

[41] Wang H, Ma L, Gan M, Zhou T, Sun X, Dai W, Wang H, Wang S (2016) Design and assembly of reduced graphene oxide/polyaniline/urchinlike mesoporous TiO2 spheres ternary composite and its application in supercapacitors. Compos Part B-Eng 92:405–412

[42] Liu L, Yang J, Jiang Y, Huang Y, Meng Q (2013) The structure characteristic and electrochemical performance of graphene/polyaniline composites. Synth Met 170:57–62

[43] Wang X, Deng J, Duan X, Liu D, Guo J, Liu P (2014) Crosslinked polyaniline nanorods with improved electrochemical performance as electrode material for supercapacitors. J Mater Chem A 2:12323–12329

[44] Yan J, Wei T, Shao B, Fan Z, Qian W, Zhang M, Wei F (2010) Preparation of a graphene nanosheet/polyaniline composite with high specific capacitance. Carbon 48:487–493

[45] Pouget JP, Józefowicz ME, Epstein AJ, Tang X, MacDiarmid AG (1991) X-ray structure of polyaniline. Macromolecules 41:779–789

[46] Liu H, Zhang W, Song H, Chen X, Zhou J, Ma Z (2014) Tremella-like graphene/polyaniline spherical electrode material for supercapacitors. Electrochim Acta 146:511–517

[47] Ramana GV, Srikanth VVSS, Padya B, Jain PK (2014) Carbon nanotube-polyaniline nanotube core-shell structures for electrochemical applications. Eur Polym J 57:137–142

[48] Marmisollé WA, Azzaroni O (2016) Recent developments in the layer-by-layer assembly of polyaniline and carbon nanomaterials for energy storage and sensing applications. From synthetic aspects to structural and functional characterization. Nanoscale 8:9890–9918

[49] Qiu H, Han X, Qiu F, Yang J (2016) Facile route to covalently-jointed graphene/polyaniline composite and it's enhanced electrochemical performances for supercapacitors. Appl Surf Sci 376:261–268

[50] Li M, Xiang S, Chang X, Chang C (2016) Resorcinol-formaldehyde carbon spheres/polyaniline composite with excellent electrochemical performance for supercapacitors. J Solid State Electrochem. doi:10.1007/s10008-016-3390-5

[51] Sing KSW, Everett DH, Haul RAW, Moscou L, Pierotti RA, Rouquérol J, Siemieniewska T (1985) Reporting physisorption data for gas/solid systems with special reference to the determination of surface area and porosity. Pure Appl Chem 57:603–619

[52] Yang ZC, Tang CH, Gong H, Li X, Wang J (2013) Hollow spheres of nanocarbon and their manganese dioxide hybrids derived from soft template for supercapacitor application. J Power Sour 240:713–720

[53] Shen K, Ran F, Zhang X, Liu C, Wang N, Niu X, Liu Y, Zhang D, Kong L, Kang L, Chen S (2015) Supercapacitor electrodes based on nano-polyaniline deposited on hollow carbon spheres derived from cross-linked co-polymers. Synth Met 209:369–376

[54] Wu Q, Xu Y, Yao Z, Liu A, Shi G (2010) Supercapacitors based on flexible graphene/polyaniline nanofiber composite films. ACS Nano 4:1963–1970

[55] Choi BG, Hong J, Hong WH, Hammond PT, Park HS (2011) Facilitated ion transport in all-solid-state flexible supercapacitors. ACS Nano 5:7205–7213

[56] Zhao D, Guo X, Gao Y, Gao F (2012) An electrochemical capacitor electrode based on porous carbon spheres hybrided with polyaniline and nanoscale ruthenium oxide. ACS Appl Mater Interfaces 4:5583–5589

[57] Gao Z, Wang F, Chang J, Wu D, Wang X, Wang X, Xu F, Gao S, Jiang K (2014) Chemically grafted graphene-polyaniline composite for application insupercapacitor. Electrochim Acta 133:325–334

[58] Yan J, Tong W, Fan Z, Qian W, Zhang M, Shen X, Wei F (2010) Preparation of graphene nanosheet/carbon nanotube/polyaniline composite as electrode material for supercapacitors. J Power Sour 195:3041–3045

[59] Luo Y, Kong D, Jia Y, Luo J, Lu Y, Zhang D, Zhang D, Qiu K, Li CM, Yu T (2013) Self-assembled graphene@PANI nanoworm composites with enhanced supercapacitor performance. RSC Adv 3:5851–5859